Simulations of the Yawed MEXICO Rotor Using a Viscous-Inviscid Panel Method

Ramos García, Néstor; Sørensen, Jens Nørkær; Shen, Wen Zhong

Published in:
Journal of Physics: Conference Series (Online)

Link to article, DOI:
10.1088/1742-6596/524/1/012026

Publication date:
2014

Document Version
Publisher's PDF, also known as Version of record

Simulations of the Yawed MEXICO Rotor Using a Viscous-Inviscid Panel Method

2014 J. Phys.: Conf. Ser. 524 012026

(http://iopscience.iop.org/1742-6596/524/1/012026)

Simulations of the Yawed MEXICO Rotor Using a Viscous-Inviscid Panel Method

N. Ramos-García, J. N. Sørensen, and W. Z. Shen
Department of Wind Energy, Fluid Mechanics Section, Building 403, Technical University of Denmark, DK-2800 Lyngby Denmark

E-mail: nerga@dtu.dk

Abstract. In the present work the viscous-inviscid interactive model *MIRAS* is used to simulate flows past the MEXICO rotor in yawed conditions. The solver is based on an unsteady three-dimensional free wake panel method which uses a strong viscous-inviscid interaction technique to account for the viscous effects inside the boundary layer. Calculated wake velocities have been benchmarked against field PIV measurements, while computed blade aerodynamic characteristics are compared against the load calculated from pressure measurements at different locations along the blade span. Predicted and measured aerodynamic forces are in overall good agreement, however discrepancies appear in the root region which could be related to an underestimation of the rotational effects arising from Coriolis and centrifugal forces. The predicted wake velocities are generally in good agreement with measurements along the radial as well as the axial traverses performed during the experimental campaign.

1. Introduction

MIRAS, a computational model for predicting the aerodynamic behavior of wind turbine rotors and its wakes has been recently developed at DTU Wind Energy by Ramos-García et al., [1] [2]. The model is based on an unsteady three-dimensional panel method following Hess approach [3], in which a distribution of singularity elements is used to model a solid body submerged in a flow field. In this way, unlike Navier-Stokes codes that need to solve the entire flow domain, panel methods avoid restrictive pre-processing and computational costs, making more attractive its use during the design stage of a wind turbine. Panel methods are rising as an alternative tool to the Blade Element Momentum (BEM) technique giving a more detailed aerodynamic description of the flow problem and at a much lower computational cost than the Navier-Stokes solvers.

The model uses a surface distribution of quadrilateral sources and doublets with a Neumann condition of no penetration as the boundary condition and a vortex filament free wake to represent the vorticity released by the blades. The method becomes even more attractive by the possibility of taking into account the viscous effects inside the boundary layer, solving the integral boundary layer equations and therefore calculating the transpiration velocity distribution [4], which is used in the viscous-inviscid coupling procedure. The viscous effects play a very important role in the blade aerodynamics, especially at low Reynolds numbers and at high angles of attack just before and after boundary layer separation takes place. In *MIRAS* the viscous effects are introduced by a coupling through angle of attack with the boundary layer solver Q^3UIC, [5].

The aim of the present work is to extensively validate the *MIRAS* code for flows past the yawed MEXICO rotor. Calculated wake velocities are benchmarked against field PIV measurements, while computed blade aerodynamic characteristics are compared against the integrated loads from pressure measurements at different span-wise locations along the blade.

2. Numerical method and governing equations

2.1. Unsteady three-dimensional free wake panel method

To simulate the flow around a wind turbine rotor, we use a viscous-inviscid coupling method where the inviscid flow is solved using an unsteady three-dimensional panel method to simulate the blades. The wake is modeled by vortex filaments clustered in vortex elements which are released at the blade trailing edges and convected downstream using the Biot-Savart law. In the following paragraphs a brief introduction to this approach will be given. For more detailed information about the model, the reader is referred to the authors' previous work [1] [2].

For a potential flow around a solid body with surface S, the velocity at a point P in the flow domain can be expressed as a superposition of the undisturbed velocity, $\mathbf{U}_\infty$, and the disturbance velocity created by the solid body, $\mathbf{U_p}$,

$$\mathbf{U}_I = \mathbf{U}_\infty + \mathbf{U}_p \tag{1}$$

In the rotating case the undisturbed velocity reads,

$$\mathbf{U}_\infty = \sqrt{(\Omega r)^2 + (\mathbf{Q}_w)^2} = \mathbf{U}_{rel} \tag{2}$$

where r is the spanwise position, Ω is the rotational velocity and $\mathbf{Q}_w$ is the wind speed.

If the flow is considered to be incompressible, inviscid and irrotational, $\mathbf{U}_p$ can be expressed as,

$$\mathbf{U}_p = -\nabla\phi \tag{3}$$

where ϕ is a potential function that satisfies the Laplace equation,

$$\nabla^2\phi = 0 \tag{4}$$

As the solid body surface S is impermeable, the normal component of the velocity must be zero at the wall which gives a Neumann condition of no penetration across the body,

$$\frac{\partial\phi}{\partial n} = \nabla\phi \cdot \mathbf{n} = \mathbf{U}_\infty \cdot \mathbf{n} \tag{5}$$

In practice, the problem is considered in two regions: the solid body and the downstream wake. The body is simulated by a distribution of quadrilateral surface dipoles, μ, and quadrilateral sources, σ. An extra source distribution, σ_{wT}, equal to the transpiration velocity, is introduced to account for viscous effects confined inside the boundary layer. The first row of wake elements is simulated using quadrilateral panel dipoles while further downstream the panels are converted into wake elements formed by straight line vortex filaments, Γ.

$$\nabla\Phi = \frac{-1}{4\pi}\int_b (\sigma + \sigma_{wT})\,\nabla\left(\frac{1}{\mathbf{r}}\right) + \frac{1}{4\pi}\int_b \mu\nabla\left[\frac{\partial}{\partial n}\left(\frac{1}{\mathbf{r}}\right)\right] + \frac{1}{4\pi}\int_w \Gamma\,\nabla\left[\frac{\partial}{\partial n}\left(\frac{1}{\mathbf{r}}\right)\right] - \nabla\Phi_\infty \tag{6}$$

The unsteady Kutta-Joukowsky condition of zero trailing edge loading is used to release the vortex filaments at the body's trailing edge. To satisfy this condition, at each time step a

quadrilateral panel with a doublet distribution is created as the first wake panel for each spanwise station. The strength of this panel, Γ_{fst}, is equal to the difference between the corresponding upper and lower trailing edge quadrilateral doublets,

$$\Gamma_{fst} = \mu_u - \mu_l \tag{7}$$

Following Katz and Plotkin [6] the first wake panel is convected downstream from the trailing edge with a 30% of the local undisturbed velocity. Downstream of the first row of wake panels the quadrilateral doublets are transformed into vortex filaments and clustered into vortex elements. The strengths of the vortex filaments remain constant in time with their motion represented by Lagrangian fluid markers placed at their end points which are convencted downstream with the total velocity $\underline{\mathbf{u}}$,

$$\mathbf{u} = \mathbf{u}_\infty + \mathbf{u}_{body} + \mathbf{u}_{wake} \tag{8}$$

where $\mathbf{u}_\infty$ is the freestream velocity, $\mathbf{u}_{body}$ is the influence of the solid body and $\mathbf{u}_{wake}$ is the induction created by the other wake elements.

The velocity induced by the wake vortex filaments is computed by applying the Biot-Savart law. In order to desingularize its behavior as $\mathbf{r}$ tends to zero, a viscous core is applied to all released vortex filaments during the time updating procedure [7]. In this way an approximation to viscous diffusion, vortex core growth and vortex straining can be included. The Biot-Savart formula is modified as follows,

$$\mathbf{u}_{wake} = K\frac{\Gamma}{4\pi}\frac{\mathbf{dl}\times\mathbf{r}}{|\mathbf{r}|^3} \tag{9}$$

where K is the kernel parameter, which uses the Scully profile for the vortex filament viscous core [8]. To include the core growth rate, Squire model is applied by introducing the turbulent eddy viscosity parameter [9]. Bhagwat et al. straining model is used to take into account variations in vortex filament radius due to filament stretching or squeezing [10].

A new solution for the solid body singularities is calculated using the influence from the updated wake geometry. The inviscid perturbation velocities are calculated on the body surface using a nodal interpolation of the doublets strength, μ. Finally, the unsteady Bernoulli equation is used to compute the surface pressure on each element on the rotor blade,

$$\frac{\partial\phi}{\partial t} + \frac{1}{2}|\mathbf{v}|^2 + \frac{1}{\rho}p = \frac{1}{\rho}p_{ref} + \frac{1}{2}|\mathbf{v}_{ref}|^2 \tag{10}$$

where $\mathbf{v}$ is the total velocity vector, p_{ref} is the far-field reference pressure and $\mathbf{v_{ref}}$ is the reference velocity, which in the rotating case is defined as follows

$$\mathbf{v}_{ref} = -\left[\mathbf{V_0} + \mathbf{\Omega}\times\mathbf{r}\right] \tag{11}$$

2.2. Viscous-inviscid coupling

The viscous boundary layer is solved in a strip manner by using the in-house Q^3UIC code [5] [11]. The Quasi-3D Unsteady Interactive Code, Q^3UIC, is an aerodynamic tool developed for solving the quasi three-dimensional integral boundary layer equations by means of a strong viscous-inviscid coupling with a two-dimensional panel method. In the inviscid part, the airfoil geometry is represented by a surface distribution of constant sources and a parabolic vorticity distribution. The viscous part is taken into account by solving the integral form of the boundary layer $r-$ and $\theta-$ momentum equations with extensions for three-dimensional rotational effects, induced by Coriolis and centrifugal forces.

The coupling between the viscous and inviscid parts in the $MIRAS$ code is achieved through the local angle of attack and the transpiration velocity as coupling parameters. Q^3UIC resolves the boundary layer, calculating the chordwise distribution of the transpiration velocity at each spanwise station along the blade, Equation 12, where δ_1^* is the streamwise displacement thickness and u_e is the boundary layer edge velocity. Q^3UIC computations are performed for a given local airfoil geometry and the following non-dimensional parameters: Reynolds number, $Re = \sqrt{(\Omega r)^2 + (Q_w)^2}\, c/\nu$, ratio between rotational speed and relative velocity, $R_O = \Omega r/U_{rel}$, local ratio between chord length and radial position, $l = c/r$, and local angle of attack, α.

$$w_T = \frac{1}{\rho}\frac{\partial}{\partial s}\left(\rho u_e \delta_1^*\right) \tag{12}$$

The computed transpiration velocity is introduced into the inviscid three-dimensional panel method as an extra quadrilateral surface source distribution, which will move outwards the limiting streamlines around the blades, taking into account the viscous effects into the final solution to the flow problem.

3. Results

Computations of flows past the MEXICO rotor in yawed conditions have been carried out using the above introduced numerical approach. A detailed comparison against the experimental data available from the MEXICO campaign is presented in what follows.

The MEXICO experiment comprised a three-bladed wind turbine model with a diameter of 4.5 m tested in the Large Scale Low Speed Facility of the German-Dutch Wind tunnel Organization DNW with a 9.5 X 9.5 m^2 open test section. The rotor was set to rotate with a constant angular speed of 424.5 rpm. Pressure measurements in yawed flow conditions were carried out at the wind speeds of 10, 15 and 24 ms^{-1} and yaw angles of 15, 30 and 45 deg. PIV measurements were carried out at the wind speed of 15 ms^{-1} and yaw angles of +30 and −30 deg. The blades were subjected in all cases to a negative pitch of $\delta_0 = -2.3°$. For more detailed information about the MEXICO experiment campaign the reader is referred to Schepers and Snel [12].

A 20 cells span- and 50 cells chord-wise surface mesh has been used for $MIRAS$ simulations. Laminar to turbulent transition was forced at a 5% of the chord from the leading edge on both the upper and lower sides of the airfoil sections in the experiment (zig-zag tapes) as well as in the viscous simulations (boundary layer trip). In this section $MIRAS$ simulations are validated against experiments in terms of the azimuthal variation of the blade aerodynamic forces and the wake velocity field.

3.1. Aerodynamic forces

The variation of the sectional force (normal and tangential components) at four different radial locations along the blade is herein compared against measured data during a complete blade revolution. The most extreme yaw case of 45 deg at wind speeds of 15 and 24 ms^{-1} are presented and analyzed in what follows.

In Figure 1 the computed normal force at the two inboard radial positions is compared against measured data obtaining a good agreement for the 15 ms^{-1} case, with a mean absolute percentage error of approximately 16% in both cases. However, the azimuthal variation of the force is strongly underpredicted for the 24 ms^{-1} case at the $0.25R$ location, which could be related to a miss prediction of the rotational effects arising from centrifugal and Coriolis forces. Experiments suggest a delay in the separation location that gives rise to an increment in the normal component of the force. Regarding the tangential force, plotted in Figure 2, a good agreement is seen at a wind speed of 15 ms^{-1}, however large differences appear at 24 ms^{-1}, with the measured data exhibiting a very different trend in the azimuthal variation of the force.

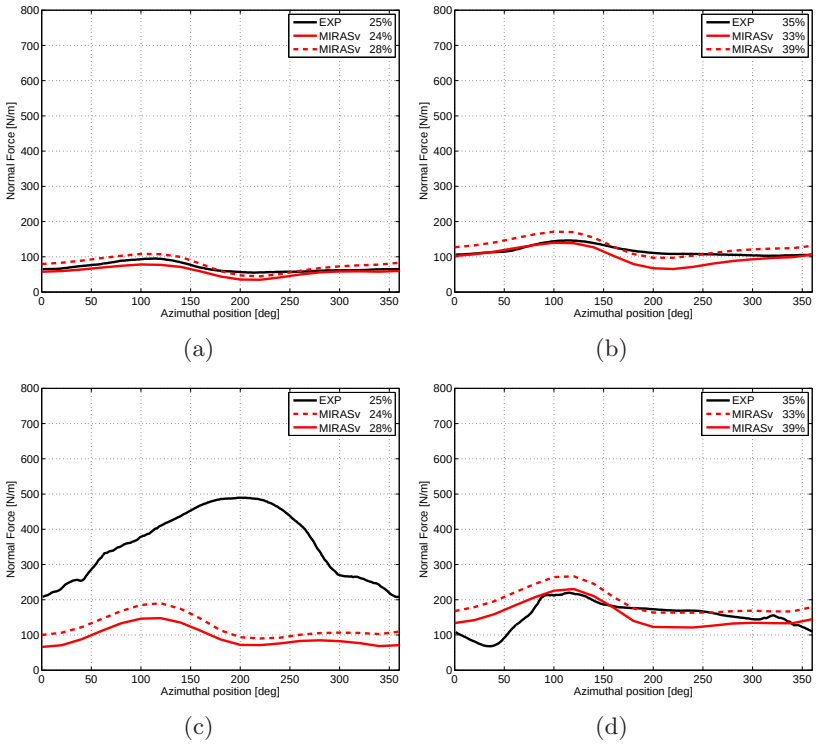

Figure 1. Normal component of the aerodynamic force in the root region of the blade, at the radial positions of (a),(c) $0.25R$, (b),(d) $0.35R$, for simulations of the flow past the MEXICO rotor at a wind speed of 15 ms^{-1} (upper) and 24 ms^{-1} (lower) and a yaw angle of 45 deg.

The computed normal force at the most outboard radial positions is compared in Figure 3 against measurements at the wind speed cases of 15 and 24 ms^{-1}. An overall good agreement is obtained at both radial locations. At a wind speed of 15 ms^{-1}, the calculated mean absolute percentage error in the predicted force at the $0.82R$ and $0.92R$ radial locations is 5.5% and 16.2% respectivelly. At a wind speed of 24 ms^{-1} the mean absolute percentage error at the respective radial locations is 9.8% and 15.8%. In Figure 4 $MIRAS$ is seen to overpredict the tangential force in the tip region although it captures correctly the azimuthal variation.

3.2. Wake velocities

PIV measurements of the flow field in the near wake of the MEXICO rotor were carried out for the yaw angles of ± 30 deg at a wind speed of 15 ms^{-1}. $MIRAS$ wake velocities are compared herein against the measured PIV data at the blade azimuthal position of 0/120 deg. Figure 5 shows the wake vortex filaments location predicted by $MIRAS$ in comparison with the tip vortex position from PIV measurements. A good agreement is obtained for for both yaw cases.

The predicted axial velocity component is compared against measurements in Figure 6. Measurements were carried out along two radial traverses, 0.15 m upstream and downstream the rotor plane. An good agreement is obtained for both yaw angles. Figure 7 shows the predicted tangential component of the velocity in comparison with measurements along the two radial traverses. The overall agreement is good. However the abrupt changes in the tip region seen during experiments are not completely captured by the numerical model. The predicted radial component of the velocity is validated in Figure 8, obtaining a good agreement with the PIV data, it is important to remark here that the peaks in the velocity created by the presence of the tip vortex and the proximity of the blade tip are well captured by the $MIRAS$ viscous solver.

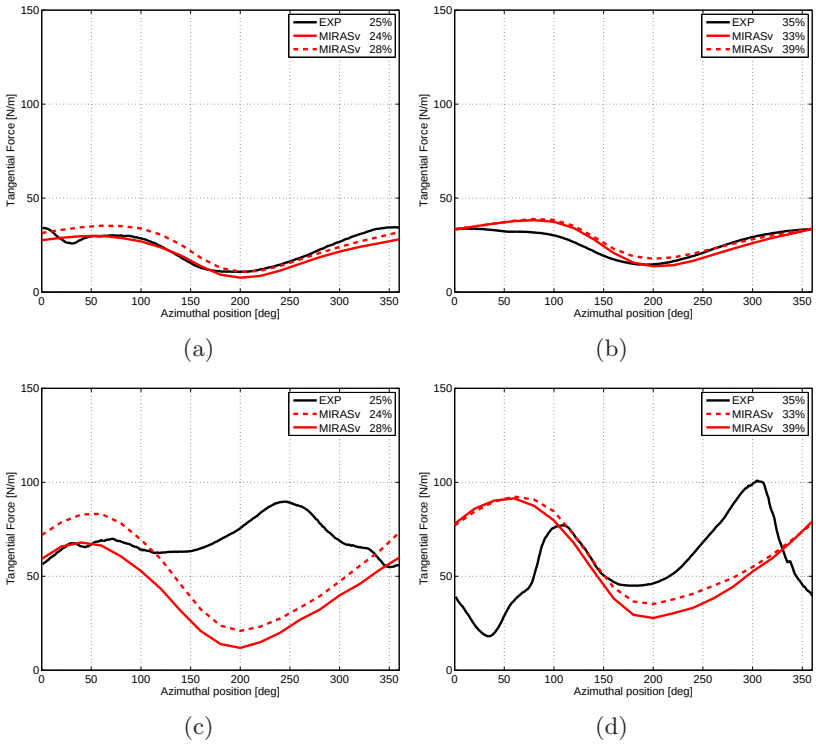

Figure 2. Tangential component of the aerodynamic force in the root region of the blade, at the radial positions of (a),(c) $0.25R$ and (b),(d) $0.35R$, for simulations of the flow past the MEXICO rotor at a wind speed of 15 ms^{-1} (upper) and 24 ms^{-1} (lower) and a yaw angle of 45 deg.

In order to compare the predicted and measured flow field further away from the rotor plane, calculated velocities are extracted along two traverses parallel to the flow direction (wind tunnel walls) at $x = 1.377\ m$ and $x = 1.848\ m$. In this case a comparison is carried out for two different yaw angles, $\pm 30\ deg$.

In Figures 9, 10 and 11 the horizontal, spanwise and vertical components of the velocity are compared against measurements for the yaw angles of $\pm 30\ deg$ at the inner radial location ($x = 1.377\ m$). From the figures it seems a better agreement between measurements and simulations for the $-30\ deg$ yaw angle, for which all three components are fairly good predicted. On the other hand, larger discrepancies appear for the positive yaw case, specially in the recovery of the horizontal wake velocities captured by experiments in Figure 9(a), which are not predicted by the model. This could be caused by the influence of the nacelle, which is not included in the numerical model.

At the outer radial position ($x = 1.838\ m$), Figures 12, 13 and 14, there is a better agreement between measurements and simulations for all three components of the velocity for both yaw angles. In this case, the recovery of the horizontal wake velocities for a positive yaw misalignment is captured by the simulations (see Figure 12(a)).

4. Conclusions

The unsteady three-dimensional interactive panel method $MIRAS$ has been validated for blade aerodynamic forces as well as wake velocity field against the MEXICO experimental data in yawed conditions. The model predicts generally good the aerodynamic forces along the complete blade span for the 15 ms^{-1} case. However, discrepancies appear at 24 ms^{-1}, especially in the root region, where $MIRAS$ underpredicts the normal forces and does not capture correctly the

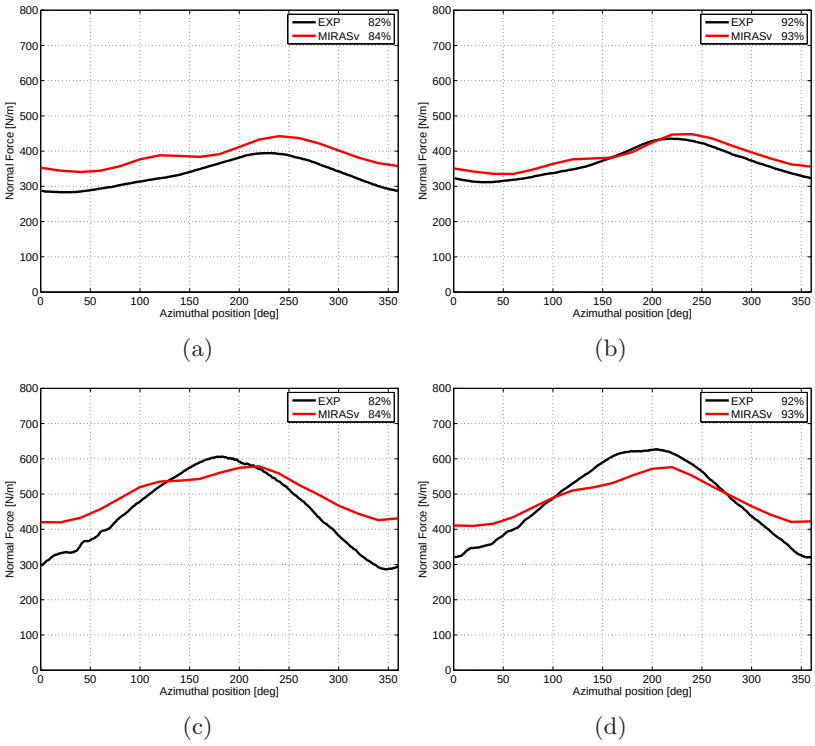

Figure 3. Normal component of the aerodynamic force in the root region of the blade, at the radial positions of (a),(c) $0.82R$, (b),(d) $0.92R$, for simulations of the flow past the MEXICO rotor at a wind speed of 15 ms^{-1} (upper) and 24 ms^{-1} (lower) and a yaw angle of 45 deg.

azimuthal variation of the tangential component seen in experiments. In terms of the velocity field, the predicted velocities are in excellent agreement with the radial traverse measurements, however some discrepancies are seen in the comparison against the axial traverse measurements for the most inner radial location. This could be due to the influence of the nacelle, which is not included in the numerical model.

5. Acknowledgements

The authors would like to acknowledge the support from the Danish Council for Strategic Research for the project 'Center for Computational Wind Turbine Aerodynamics and Atmospheric Turbulence' (2104-09-067216/DSF), the Energy Technology Development and Demonstration Program (EUDP-2011-64011-0094) and the Danish Energy Agency (EUDP-2012-64012-0146).

References

[1] N. Ramos-García, J.N. Sørensen and W.Z. Shen 2013 *Three-Dimensional Viscous-Inviscid Coupling Method for Wind turbine Computations* Submitted to Wind Energy.
[2] N. Ramos-García, J.N. Sørensen and W.Z. Shen 2014 *Validation of a three-dimensional viscous-inviscid interactive solver for wind turbine rotors* Renewable Energy: Special Issue in Wind Energy. Published online.
[3] J. L. Hess 1971 Numerical solution of inviscid subsonic flows *Von Karman Institute for Fluid Dynamics, Lecture Series* **34**
[4] M. J. Lighthill 1958 On displacement thickness *Journal of Fluid Mechanics*
[5] N. Ramos-García, J.N. Sørensen and W.Z. Shen 2013 *A Strong Viscous-Inviscid Interaction Model for Rotating Airfoils* Published online in Wind Energy.

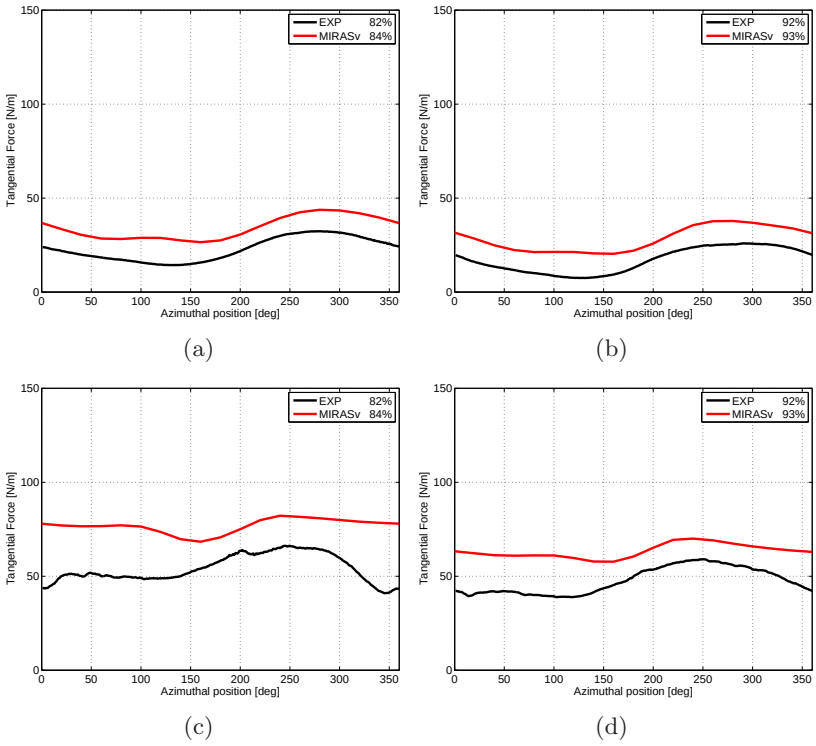

Figure 4. Tangential component of the aerodynamic force in the root region of the blade, at the radial positions of (a),(c) $0.82R$ and (b),(d) $0.92R$, for simulations of the flow past the MEXICO rotor at a wind speed of 15 ms^{-1} (upper) and 24 ms^{-1} (lower) and a yaw angle of 45 deg.

[6] J. Katz and A. Plotkin 1977 Low speed aerodynamics: from wing theory to panel methods *McGraw-Hill*
[7] J.G. Leishman, M.J. Bhagwat and A. Bagai 2002 Free-Vortex Filament Methods for the Analysis of Helicopter Rotor Wakes *Journal of Aircraft* ***5****: 759–775*
[8] M.P. Scully 1975 Computation of Helicopter Rotor Wake Geometry and Its Influence on Rotor Harmonic Airloads *Ph.D. Thesis, Massachusetts Institute of Technology. Dept. of Aeronautics and Astronautics*
[9] H.B. Squire 1965 The growth of a vortex in turbulent flow *Aeronautical Quarterly* ***16****: 302–306*
[10] M.J. Bhagwat and J.G. Leishman 2001 Accuracy of Straight-Line Segmentation Applied to Curvilinear Vortex Filaments *Journal of the American Helicopter Society* ***46****:2:166-169*
[11] N. Ramos-García, J.N. Sørensen and W.Z. Shen 2012 *A quasi-3D viscous-inviscid interaction code: Q^3UIC* Journal of Physics: Conference Series, The Science of Making Torque from Wind.
[12] J.G. Scheepers and H. Snel 2007 Model Experiments in Controlled Conditions Final Report *The Energy Research Center of the Netherlands The Energy Research Center of the Netherlands*

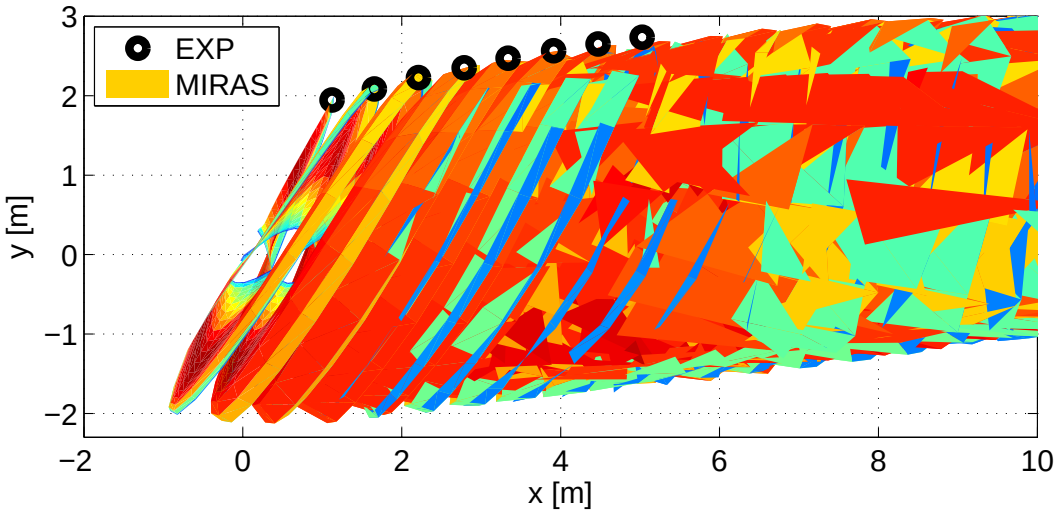

(a)

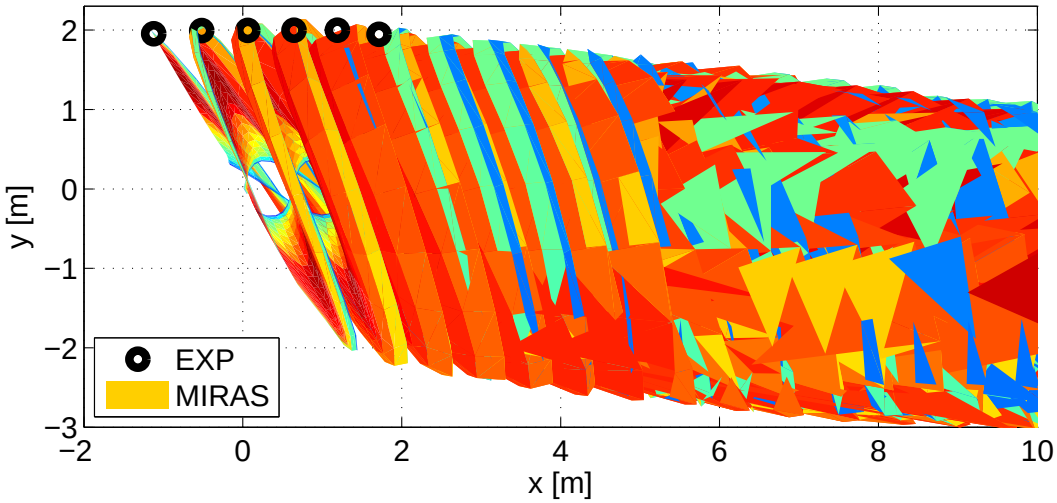

(b)

Figure 5. Tip vortex position comparison between $MIRAS$ simulations and PIV measurements at a wind speed of 15 ms^{-1} and yaw angles of (a) $+30$ deg, (b) -30 deg.

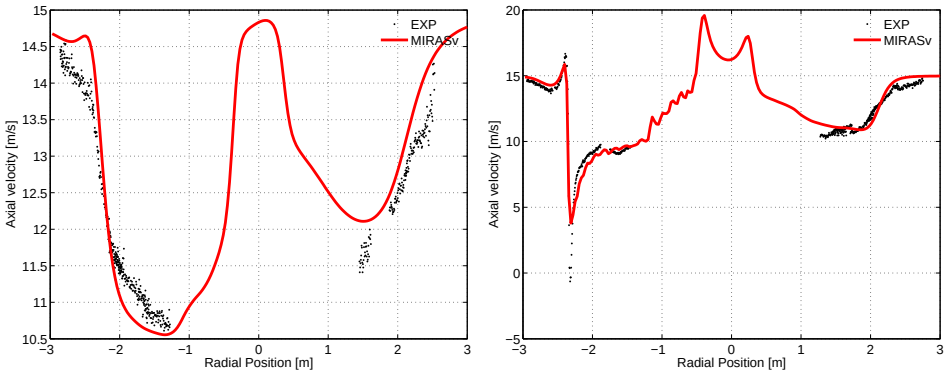

Figure 6. Axial component of the velocity for the flow past the MEXICO rotor along two radial traverses: (a) 0.15 m upstream the rotor plane (b) 0.15 m downstream the rotor plane, at a wind speed of 15 ms^{-1} and a yaw angle of 30 deg.

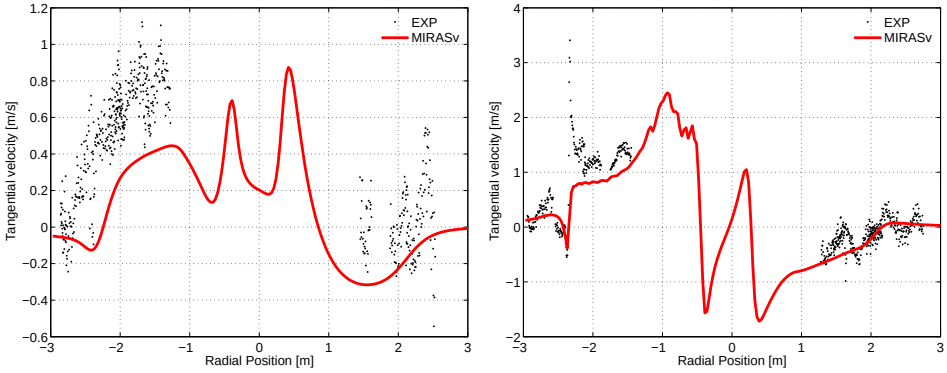

Figure 7. Tangential component of the velocity for the flow past the MEXICO rotor along two radial traverses: (a) 0.15 m upstream the rotor plane (b) 0.15 m downstream the rotor plane, at a wind speed of 15 ms^{-1} and a yaw angle of 30 deg.

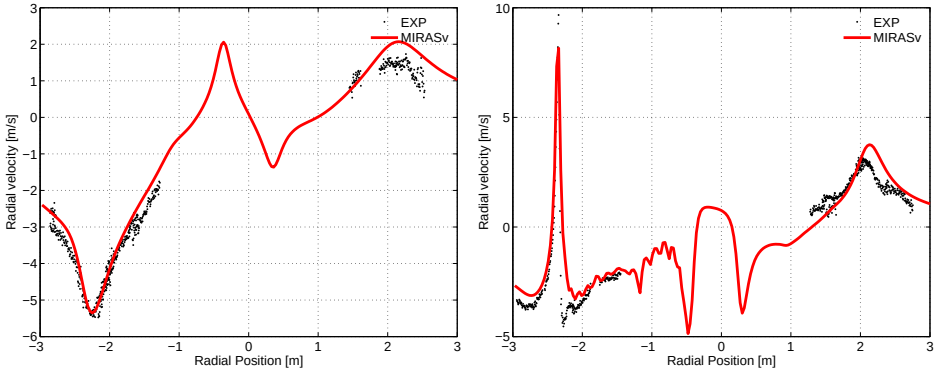

Figure 8. Radial component of the velocity for the flow past the MEXICO rotor along two radial traverses: (a) 0.15 m upstream the rotor plane (b) 0.15 m downstream the rotor plane, at a wind speed of 15 ms^{-1} and a yaw angle of 30 deg.

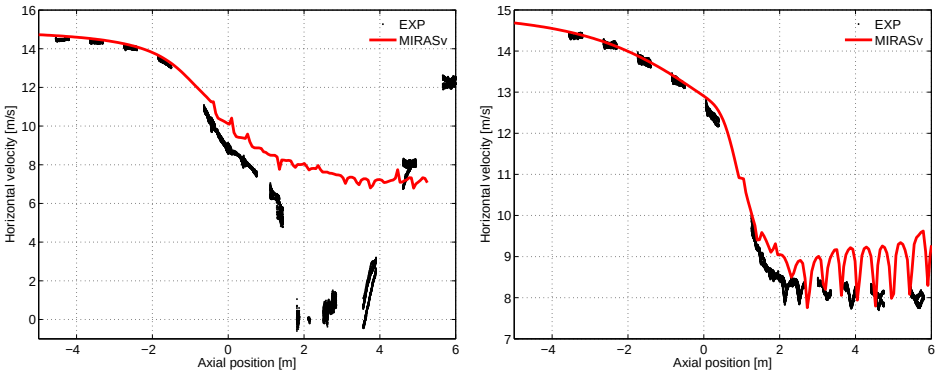

(a) (b)

Figure 9. Horizontal velocity (in wind tunnel coordinates) for the flow past the MEXICO rotor along the axial traverse at $x = 1.377\ m$, at a wind speed of 15 ms^{-1} (a) yaw angle of $+30\ deg$ (b) yaw angle of $-30\ deg$.

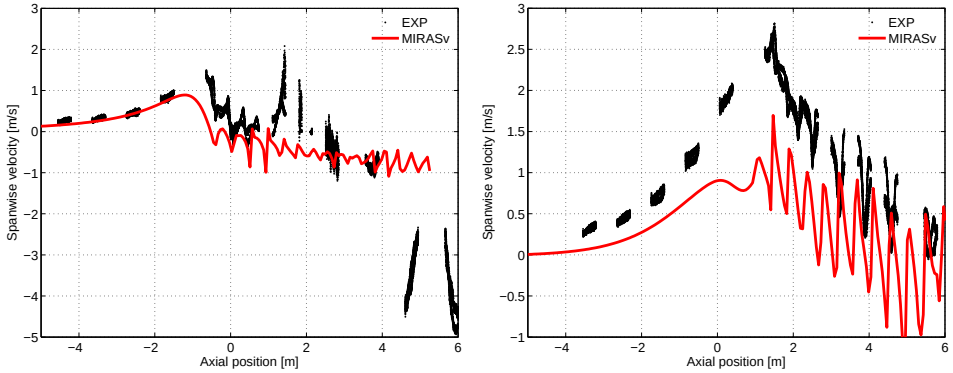

(a) (b)

Figure 10. Spanwise velocity (in wind tunnel coordinates) for the flow past the MEXICO rotor along the axial traverse at $x = 1.377\ m$, at a wind speed of 15 ms^{-1} (a) yaw angle of $+30\ deg$ (b) yaw angle of $-30\ deg$.

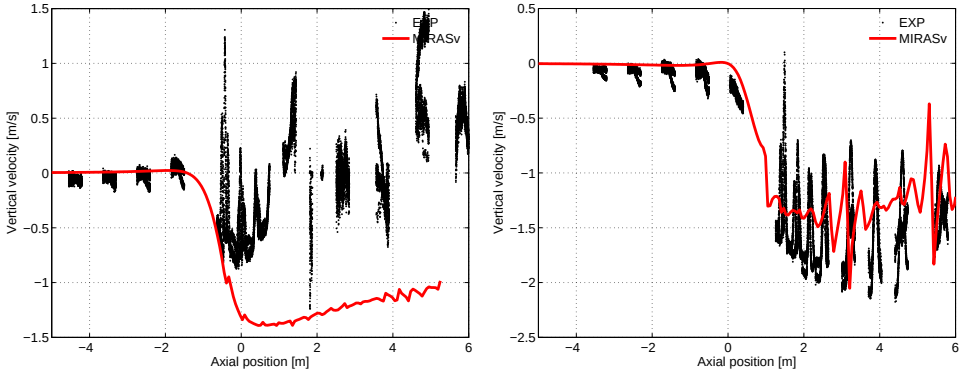

(a) (b)

Figure 11. Vertical velocity (in wind tunnel coordinates) for the flow past the MEXICO rotor along the axial traverse at $x = 1.377\ m$, at a wind speed of 15 ms^{-1} (a) yaw angle of $+30\ deg$ (b) yaw angle of $-30\ deg$.

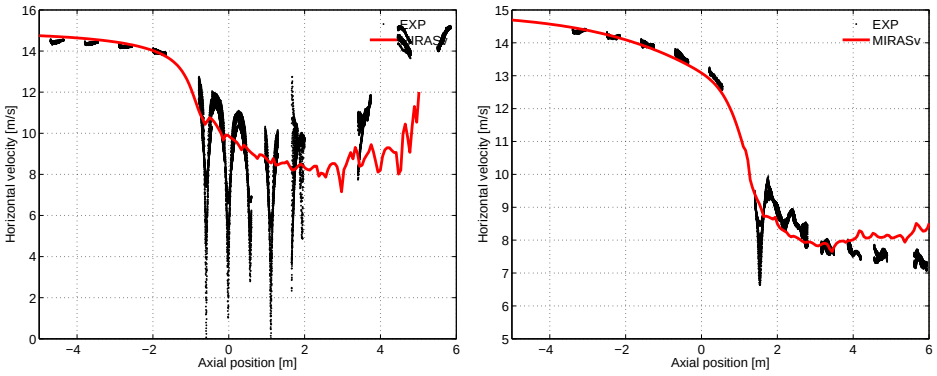

(a) (b)

Figure 12. Horizontal velocity (in wind tunnel coordinates) for the flow past the MEXICO rotor along the axial traverse at $x = 1.848\ m$, at a wind speed of 15 ms^{-1} (a) yaw angle of +30 *deg* (b) yaw angle of −30 *deg* .

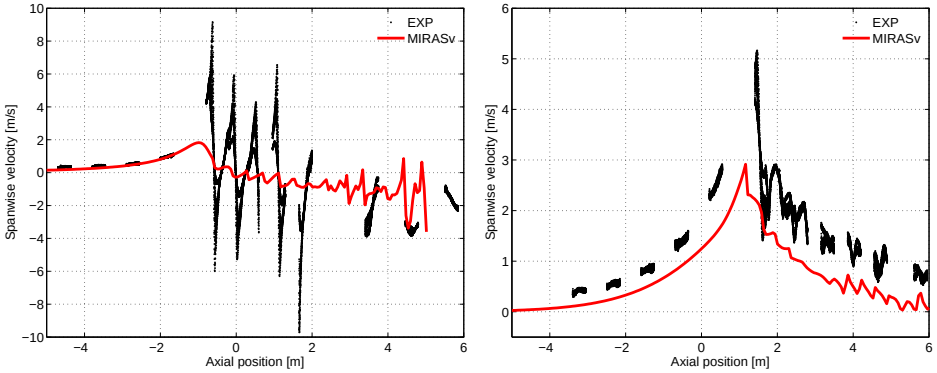

(a) (b)

Figure 13. Spanwise velocity (in wind tunnel coordinates) for the flow past the MEXICO rotor along the axial traverse at $x = 1.848\ m$, at a wind speed of 15 ms^{-1} (a) yaw angle of +30 deg (b) yaw angle of -30 deg .

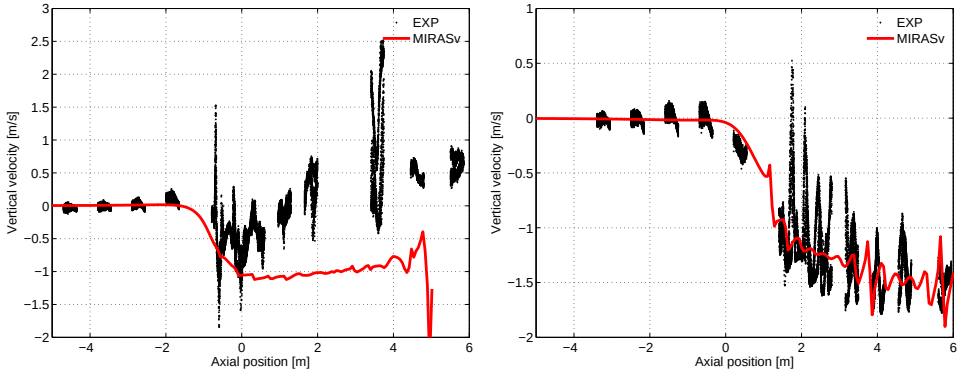

(a) (b)

Figure 14. Vertical velocity (in wind tunnel coordinates) for the flow past the MEXICO rotor along the axial traverse at $x = 1.848\ m$, at a wind speed of 15 ms^{-1} (a) yaw angle of +30 *deg* (b) yaw angle of −30 *deg* .